Guided Plasmon Modes of Elliptical Cross Section Silver Nanoridges

Zeyu Pan, *Student Member, IEEE, Student Member, OSA*, Junpeng Guo, Richard Soref, *Life Fellow, IEEE*, and Walter Buchwald

***Abstract*—Propagating two-dimensional plasmon polariton modes guided by elliptical cross section silver nanoridges are investigated in this paper. Mode field profiles, dispersion curves, propagation distances, and figure-of-merits of the plasmon modes are calculated for various elliptical cross section silver nanoridges. It is found that the elliptical cross section metal nanoridge, if designed properly, can support a tightly confined plasmon mode with a longer propagation distance and a higher figure-of-merit than the flat-top nanoridge waveguide of the same width. The optimal nanoridge waveguide is obtained when the elliptical waveguide cross section becomes a semicircular cross section. When the curvature of the elliptical nanoridge is large, the nanoridge plasmon mode approaches the wedge plasmon mode.**

***Index Terms*—Optical waveguide, surface plasmon.**

I. Introduction

SURFACE plasmons are free electron density oscillations on the metal-dielectric interfaces, and can propagate along the metal-dielectric boundaries in the form of surface plasmon polariton waves with tightly confined sub-wavelength scale modes [1]–[3]. Surface plasmon modes in various waveguide structures, such as thin metal films [4]–[8], finite width thin film metal stripes and metal wires [9]–[17], trenches in the metal surface [18]–[29], metal dielectric layer structures [30]–[39], dielectric-loaded metal films [40]–[46] and metal wedges [25], [26], [47]–[52], have been extensively investigated. The quest for strong mode confinement and low propagation attenuation waveguides has motivated research efforts on various waveguide structures. Recently, 2-D surface plasmon waveguide modes of flat-top and triangular-shape silver metal nanoridges have been numerically investigated [53], [54]. Round-top gold nanoridge plasmon waveguides have been fabricated with the focused ion beam (FIB) milling technique [52].

Manuscript received February 10, 2012; revised April 30, 2012, June 13, 2012; accepted June 16, 2012. Date of publication June 21, 2012; date of current version August 01, 2012. This work was supported in part by the National Science Foundation under Grant NSF-0814103 and by the National Aeronautics and Space Administration under Grant NNX07 AL52A. The work of J. Guo was supported by the ASEE-Air Force Office of Scientific Research Summer Faculty Fellowship Program.

Z. Pan and J. Guo are with the Department of Electrical and Computer Engineering, University of Alabama, Huntsville, AL 35899 USA (e-mail: zp0002@uah.edu; guoj@uah.edu).

R. Soref is with the Department of Physics, University of Massachusetts, Boston, MA 02125 USA (e-mail: soref@rcn.com).

W. Buchwald is with the Solid State Scientific Corporation, Hollis, NH 03049 USA (e-mail: walter.buchwald@solidstatescientific.com).

Color versions of one or more of the figures in this paper are available online at http://ieeexplore.ieee.org.

Digital Object Identifier 10.1109/JLT.2012.2205557

This paper presents comprehensive numerical investigations on the plasmon modes supported by elliptical cross section silver nanoridges. Mode field distributions, mode indices, dispersion curves, propagation distances, mode sizes, and the figure-of-merits of silver nanoridge plasmon waveguides with various surface curvatures are calculated. The motivation for investigating such elliptical cross section metal nanoridge waveguides is to find an optimal geometry that provides longer propagation distance and higher figure-of-merit. In addition, as will be shown, elliptical cross section nanoridge waveguides provide more uniform distributions of the plasmon mode fields when compared to the flat-top and wedge plasmon waveguides. This feature is important in applications requiring an expanded interaction region such as chemical and biological sensing. Elliptical cross section nanoridge plasmon waveguides can be fabricated with the focused ion beam (FIB) milling technique. FIB is a very powerful nanofabrication technique for realizing nanoscale structures and shapes in various materials [55].

II. Elliptical Cross Section Silver Nanoridge Plasmon Waveguides

The 3-D view and cross section of such an elliptical silver nanoridge waveguide are shown in Fig. 1(a) and (b), where the nano-scale metal ridge is extended in the z-direction with its width (w) in the x-direction and the half ellipse height (h) in the y-direction. The plasmon mode propagates along the ridge top in the z-direction. We assume the height of the ridge is sufficiently high that the substrate does not influence the ridge mode. The geometry of the elliptical cross section nanoridge is symmetric in x-axis, and non-symmetric in y-axis. Our previous work on the plasmon modes supported by the flat-top silver nanoridges [53] has found that a ridge width of 120 nm produces an optimal compromise between propagation distance and mode confinement. In this study, we thus fix the ridge width at 120 nm, for all elliptical cross section nanoridges investigated.

To describe the elliptical cross section, we use the curvature (κ), instead of the height (h). The curvature is the reciprocal of the radius of curvature (R). The radius of curvature at the top of the ridge is $R = w^2/4h$. Thus, the curvature at the top of the ridge is $\kappa = 1/R = 4h/w^2$.

We use a full-vectoral finite-difference mode solver [56] developed by *Lumerical Solutions, Inc.* to calculate the 2-D plasmon modes of the nanoridge plasmon waveguides. The finite-difference method uses Yee's 2-D mesh with appropriate boundary conditions to numerically solve Maxwell's equations in the frequency domain. Solving the Maxwell equations becomes a problem of solving an eigenvalue problem. The mode index is obtained by solving the eigenvalue equation.

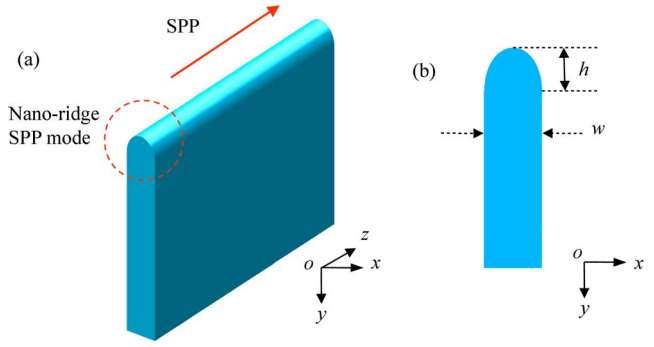

Fig. 1. (a) 3-D view of the elliptical nanoridge plasmon waveguide. (b) Cross section of the elliptical nanoridge plasmon waveguide.

We consider the situation where the surrounding medium of the nanoridges is air ($\varepsilon_d = 1.0$), and the nanoridges are made of silver with its electric permittivity $\varepsilon_m = -127.5 - 5.3j$ at the telecommunication wavelength of 1.55 μm [57]. For the flat-top ridge with a width of 120 nm, the mode effective index and the attenuation coefficient are found to be $n_{\text{eff}} = 1.018 - 0.00074j$ and 261.87 dB/cm, respectively. Although this study investigates silver as the ridge material, the analysis can obviously be extended to other types of metals and high electron density materials, such as heavily doped semiconductors [58]–[60] at different wavelengths.

We calculated the real and imaginary parts of the mode field components of the 120 nm wide elliptical silver nanoridge plasmon waveguide with $\kappa = 16.67\ \mu\text{m}^{-1}$ ($h = 60$ nm) at the 1.55 μm wavelength. We found that the real parts of E_x and E_y are three orders of magnitude larger than the imaginary parts of E_x and E_y. The real parts of H_x and H_y are two orders of magnitude larger than the imaginary parts of H_x and H_y. But the real parts of E_z and H_z are two orders of magnitude less than the imaginary parts of E_z and H_z. So, we plot the real part of E_x, the real part of E_y, and the imaginary part of E_z mode profiles in the Fig. 2(a)–(c). Also, we plot the real part of H_x, the real part of H_y, and the imaginary part of H_z mode profiles in the Fig. 2(d)–(f). It can be seen that the E_y mode profile and H_x mode profile are symmetrical with respect to the center of the metal ridge (i.e., $x = 0$ plane), while the E_x and H_y profiles are anti-symmetrical with respect to the $x = 0$ plane for such a plasmon mode propagating along the top surface of an elliptical metal ridge. The flat-top nanoridges ($\kappa = 0\ \mu\text{m}^{-1}$) have the similar symmetric properties with elliptical nanoridges [53]. The as_b^0 mode and the ss_b^0 mode of the finite width metal stripe in vacuum [10] can be considered as coupled two flat-top nanoridges located at the left and right sides of the finite width metal stripe.

We also calculated the field amplitudes of the three vectorial components of the 120 nm wide elliptical silver nanoridge plasmon waveguide with $\kappa = 16.67\ \mu\text{m}^{-1}$ ($h = 60$ nm) at the 1.55 μm wavelength. Fig. 3(a)–(c) are the mode amplitude profiles of three electric field components (E_x, E_y, E_z) at the 1.55 μm wavelength. Fig. 3(d)–(f) are the mode amplitude profiles of three magnetic field components (H_x, H_y, H_z) of the elliptical nanoridge waveguide at the same wavelength. It can be seen that the major components of the electric field are in

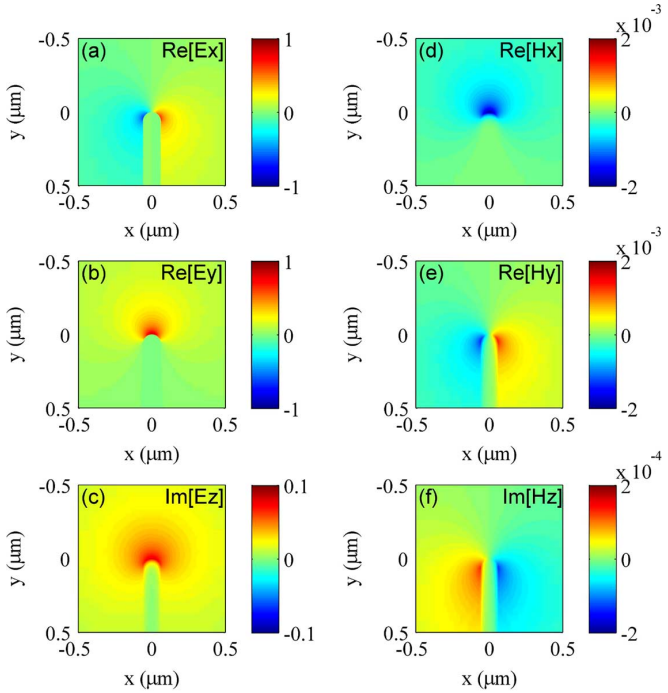

Fig. 2. Mode profiles at 1.55 μm wavelength: (a) real part of the electric field E_x, (b) real part of the electric field E_y, (c) imaginary part of the electric field E_z, (d) real part of the magnetic field H_x, (e) real part of the magnetic field H_y, and (f) imaginary part of the magnetic field H_z.

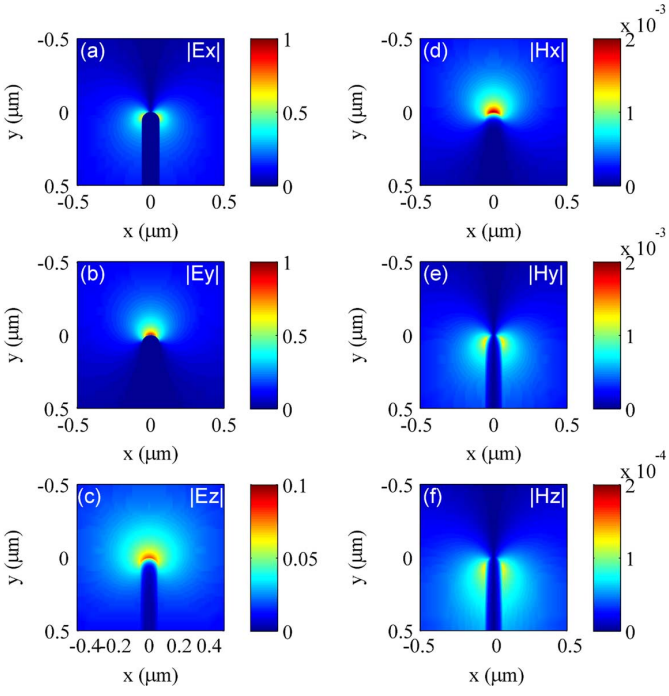

Fig. 3. (a)–(c) Electric field (E_x, E_y, E_z) amplitude mode profiles of an elliptical silver nanoridge with $\kappa = 16.67\ \mu\text{m}^{-1}$ ($h = 60$ nm) at 1.55 μm wavelength. (d)–(f) Magnetic field (H_x, H_y, H_z) amplitude mode profiles of the silver nanoridge with $\kappa = 16.67\ \mu\text{m}^{-1}$ ($h = 60$ nm) at 1.55 μm wavelength.

the transverse directions, which are about one order of magnitude larger than the longitudinal component of the electric field E_z. The major magnetic field components are also in the transverse directions, which are one order of magnitude larger than

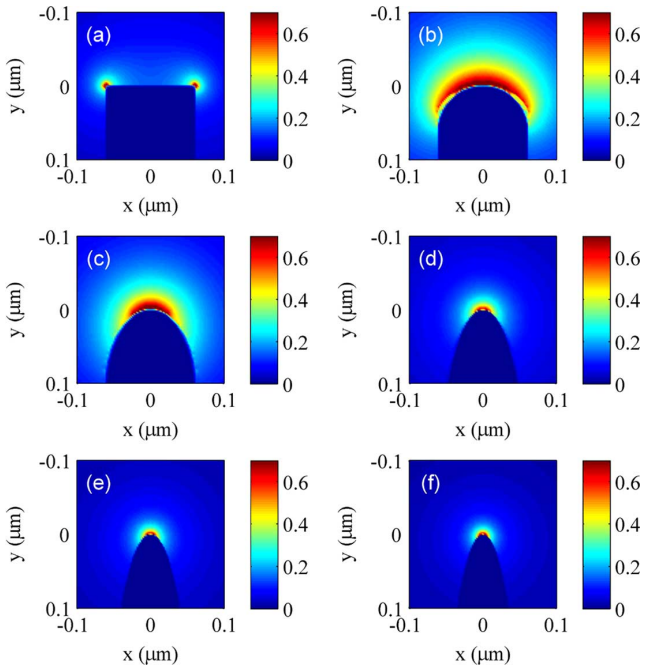

Fig. 4. Electric field intensity distributions of the 120 nm wide elliptical nanoridge plasmon waveguide with curvature equal to (a) 0 μm^{-1}, (b) 15 μm^{-1}, (c) 30 μm^{-1}, (d) 70 μm^{-1}, (e) 110 μm^{-1}, and (f) 150 μm^{-1} at 1.55 μm wavelength.

the longitudinal component of the magnetic field H_z. Therefore, the elliptical cross section nanoridge plasmon mode can be considered as a quasi-transverse electromagnetic (TEM) mode.

We calculated the electric field intensity distributions of the fundamental plasmon propagating modes supported by elliptical nanoridges of different curvatures at the wavelength of 1.55 μm with width of the nanoridges set to 120 nm in all cases. Fig. 4(a) shows that the electric field intensity distribution of the flat-top nanoridge has two hot spots located at each corner of the ridge, which can be considered as a hybrid mode of two 90° wedge plasmon modes first described in [53]. Fig. 4(b)–(f) shows the electric field intensity distributions of the elliptical nanoridge plasmon modes with the curvature of 15 μm^{-1}, 30 μm^{-1}, 70 μm^{-1}, 110 μm^{-1}, and 150 μm^{-1}, respectively. It can be seen that for the elliptical nanoridge with a curvature between 9 and 18 μm^{-1}, the mode spans the entire ridge. As the curvature increases, the mode progressively converges towards the tip of the ellipse with increasing mode confinement. As the curvature increases to above 18 μm^{-1}, the mode converges to only one hot spot at the top of the ridge, which can be considered as a small angle wedge mode. We also find that the mode energy is distributed over the entire ridge when the curvature is small. In this case, the elliptical nanoridge mode is seen to be insensitive to the change of curvature. However, once the curvature becomes greater than 18 μm^{-1}, the mode is seen to be concentrated at the top of the elliptical ridge, and is seen to rapidly intensify with the increasing curvature. It also can be seen that the plasmon mode of the rounded finite width metal strip [13] can be considered as the coupled two elliptical nanoridge modes located at the left and right sides of the metal stripe.

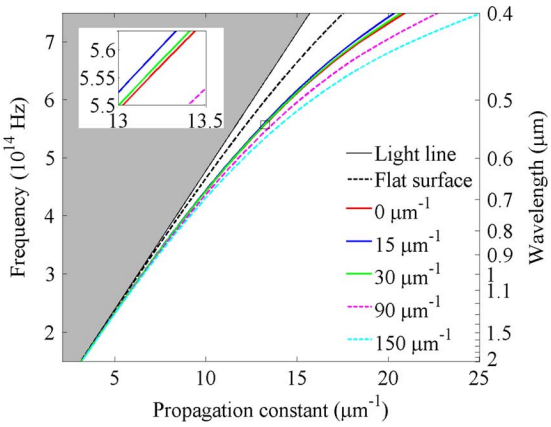

Fig. 5. Dispersion curves of the silver elliptical nanoridge plasmon waveguides of different curvatures and the comparison with the dispersion curve of the silver-air flat surface plasmon mode.

The mode dispersion curves of elliptical silver nanoridges of different curvatures are calculated and shown in Fig. 5. The black solid line is the light line in air. The black dashed line is the plasmon dispersion curve associated with the silver-air flat interface. In this figure, for all the curvatures, as the frequency increases, the plasmon mode dispersion curves drift away from the light line in air, suggesting slower group velocity and tighter mode confinement. This effect is far more pronounced for ridges with larger curvature. This is in contrast to the effects of the curvature on the dispersion curve, which is more easily seen in the inset of Fig. 5. Here, as the curvature increases from zero (i.e., the flat-top nanoridge), the dispersion curve first moves toward the light line (i.e., to the left side of the flat-top nanoridge dispersion curve in the inset), indicating a reduction in mode confinement. Once the curvature increases above 16.67 μm^{-1}, the dispersion curve moves away from the light line and eventually falls in the right side of the zero curvature case, indicating the increase of both the mode confinement and propagation attenuation. The red line is the dispersion curve of the flat-top nanoridge waveguide. The blue line is the dispersion curve of the nanoridge waveguide with 15 μm^{-1} curvature. The green line is the dispersion curve of the nanoridge waveguide with 30 μm^{-1} curvature. The magenta and cyan dashed lines are the dispersion curves of the nanoridge waveguides with the curvature of 90 μm^{-1} and 150 μm^{-1}, respectively. It is also seen that the dispersion curves of ridges with curvatures between 9 and 18 μm^{-1} are relatively insensitive to curvature changes. While beyond a curvature of 18 μm^{-1}, the mode intensity is more concentrated to the tip of the elliptical ridge. The dispersion curve moves rapidly away from the light line when the curvature of the elliptical ridge continues to increase, and the ridge plasmon mode gradually approaches a wedge plasmon mode.

The real and imaginary parts of the elliptical nanoridge mode index versus the wavelength for several different curvatures (κ = 0 μm^{-1}, 15 μm^{-1}, 30 μm^{-1}, 90 μm^{-1}, and 150 μm^{-1}) are plotted in Fig. 6, where the black dashed lines are those of the silver-air flat plasmon mode. As the wavelength increases, both the real and imaginary parts of the elliptical nanoridge mode index decrease, indicating a reduction in the mode confinement as well as the propagation loss. We can also

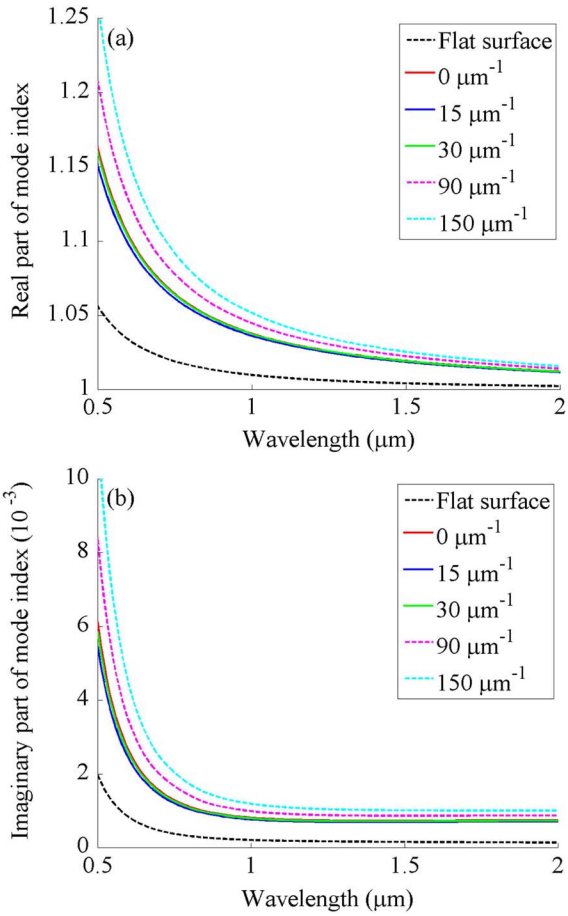

Fig. 6. (a) Real part and (b) imaginary part of the mode index versus the wavelength for different curvatures and the comparison with those of the silver-air flat plasmon mode index.

see when the curvature increases from the zero, both the real and imaginary part of the elliptical nanoridge mode index first reduce, and further increase of the curvature increases those of the elliptical nanoridge mode index, which is consistent with the results shown in Figs. 4 and 5.

The real and imaginary parts of the mode index versus the curvature at 1.55 μm wavelength are shown in Fig. 7. Interestingly, both the real and imaginary parts of the elliptical nanoridge mode index are first seen to decrease with an initial increase in the elliptical curvature, indicating a reduction in propagation attenuation and mode confinement, however, after reaching minimum values at 16.67 μm^{-1}, rapid increase in both real and imaginary parts of the mode index is observed, which corresponds to a quick rise in both attenuation and confinement. It is interesting to note that considering the 120 nm ridge width here, a semi-circle of 60 nm radius would have a curvature of 16.67 μm^{-1}. This suggests that a semicircular geometry is the optimal for reduced propagation loss and increased mode confinement.

In general, the propagation of surface plasmon modes can be characterized by a complex wave vector of the form $\beta_z = n_{\text{eff}} k_0 = \beta - j\alpha$, along the z-direction, where β is the phase propagation constant of the mode, and α is the attenuation constant. The propagation distance is defined as the distance where the mode intensity attenuates to $1/e$ of its initial value, i.e., $L_p = 1/(2\alpha)$. The propagation distances are calculated

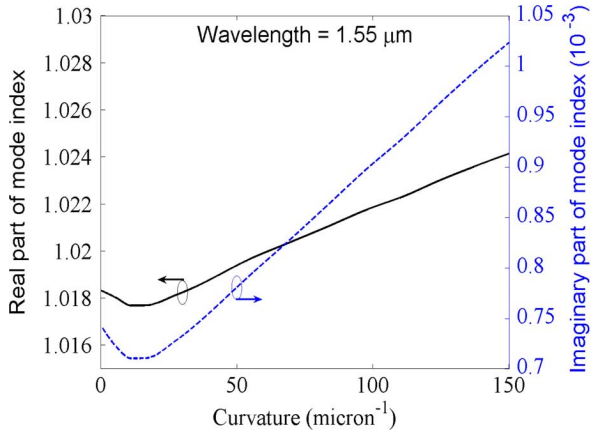

Fig. 7. Real and imaginary parts of the mode index versus the curvature at 1.55 μm wavelength.

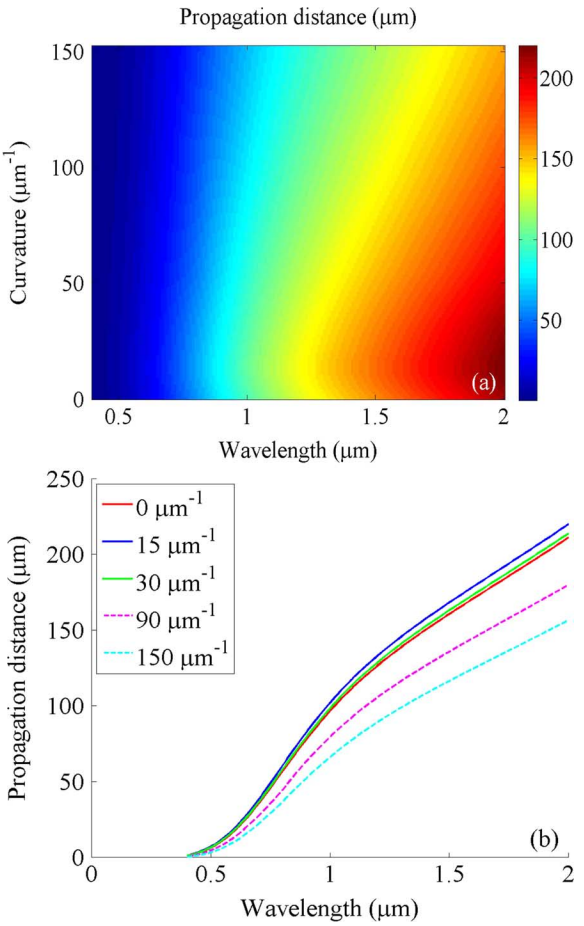

Fig. 8. (a) Propagation distance versus the wavelength and the curvature. (b) Propagation distance of the elliptical nanoridge mode versus the free space wavelength for different curvatures.

for the elliptical nanoridge plasmon waveguide at different curvatures and different free space wavelengths. The results are shown in Fig. 8(a) and (b). It can be seen that at any given wavelength as the curvature increases, the propagation distance first increases, and then reaches plateau for curvature between 9 and 18 μm^{-1}, after which it is seen to decrease rather rapidly. As the wavelength increases, the propagation distance also increases. As discussed in the [26], for the wedge plasmon mode,

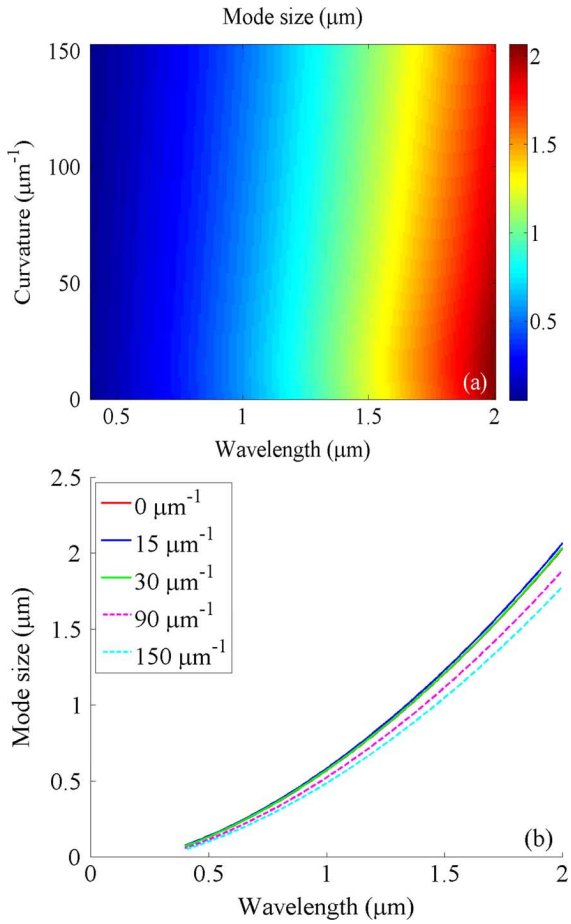

Fig. 9. (a) Mode size versus the wavelength and curvature. (b) Mode size of the elliptical nanoridge plasmon mode versus the free space wavelength for different curvatures.

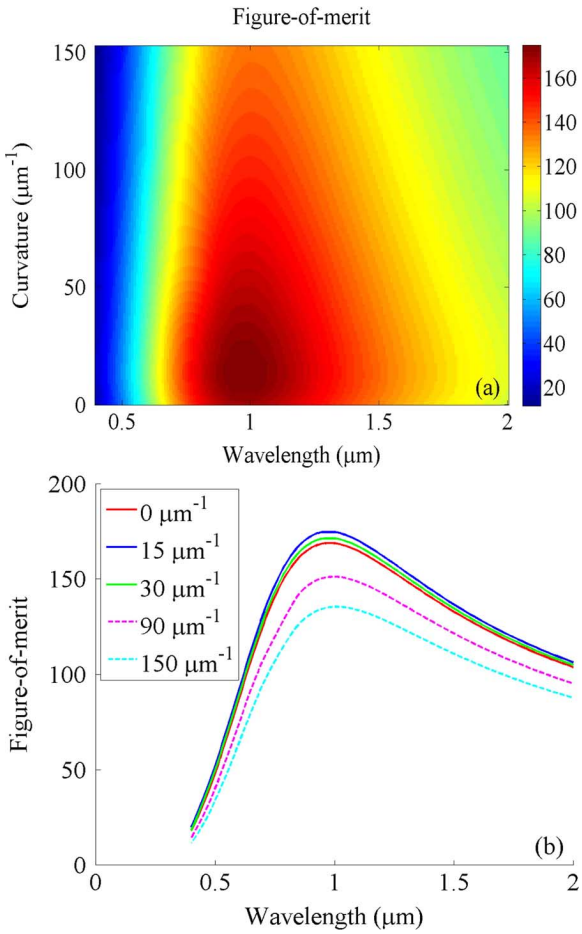

Fig. 10. (a) Figure-of-merit versus the wavelength and the curvature. (b) Figure-of-merit versus the wavelength for several curvatures.

the propagation loss increases dramatically as the wedge angle decreases. When the curvature is between 9 and 18 μm^{-1}, it appears that the mode energy is distributed more evenly along the entire ridge, and the associated nanoridge plasmon mode can be considered as an infinite number of coupled large-angle wedge plasmon modes. Within this curvature range, these coupled wedge plasmon modes of the elliptical nanoridge have smaller loss, so the nanoridge plasmon mode has the longest propagation distance.

Outside the metal ridge in the surrounding dielectric medium, the transverse component of the complex wave vector is given by $\beta_\perp = \gamma - j\delta$, where γ and δ describe the field oscillation and decay in the transverse direction, respectively. It follows from Maxwell's equations that the complex propagation constants in the propagation direction and the transverse directions are related as

$$(\beta - j\alpha)^2 + (\gamma - j\delta)^2 = \varepsilon_d k_o^2 \tag{1}$$

where k_0 is the mode propagation constant in the free space, and ε_d is the dielectric constant of the surrounding dielectric. Solving (1), we can obtain γ and δ, which are used to define the mode size as $1/2\delta + 1/2\delta = 1/\delta$. The mode size versus the free space wavelength and the ellptical curvature is shown in Fig. 9(a), while Fig. 9(b) shows the mode size versus the free space wavelength at various elliptical curvatures. Here it is seen that the mode size increases as the wavelength increases. Once again, for the curvature smaller than 9 μm^{-1}, the mode size slightly increases, but when the curvature increases higher than 18 μm^{-1}, the mode size decreases rapidly.

While it is always desirable to obtain surface plasmon waveguides with tight confinement and low attenuation, the reality is that there is always a trade-off between the propagation attenuation and the mode confinement [12], [61]. While tight mode confinement is the merit, attenuation is the cost. Figure-of-merits have been proposed to characterize this trade-off between attenuation and mode confinement [62], [63]. Here, we define the figure-of-merit of the nanoridge plasmon waveguide as the ratio of the propagation distance over the mode size:

$$\text{FoM} = (1/2\alpha)/(1/\delta) = \delta/2\alpha. \tag{2}$$

We calculated the figure-of-merit versus the wavelength and the curvature. The results are shown in Fig. 10(a). Fig. 10(b) shows the figure-of-merit versus the wavelength for several different curvatures. It can be seen from Fig. 10(a) and (b) that the figure-of-merit reaches a maximum at the 1.05 μm wavelength for all curvatures considered in this study. It also can be seen that the magnitude of the figure-of-merit peak is related to the curvature, with values between 9 and 18 μm^{-1} producing

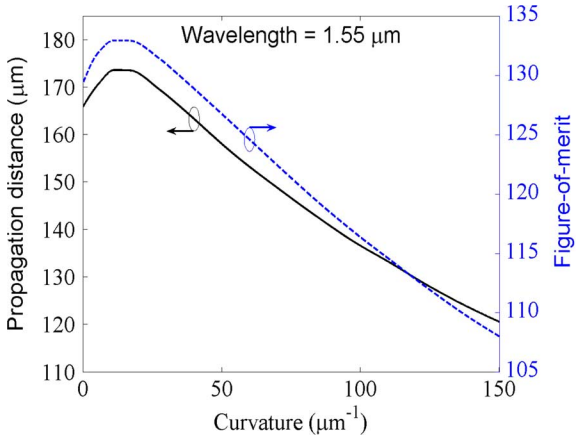

Fig. 11. Propagation distance and figure-of-merit of elliptical nanoridge waveguide mode versus the curvature at 1.55 μm wavelength.

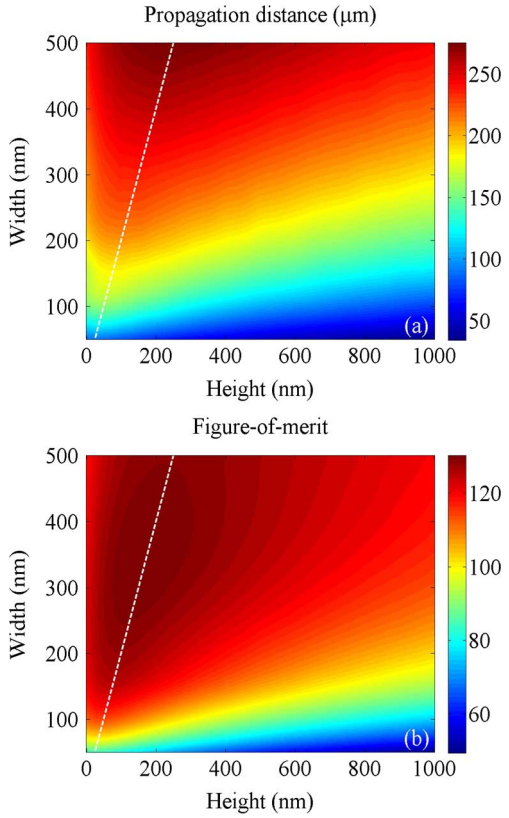

Fig. 12. Propagation distance and figure-of-merit versus the height and the width at 1.55 μm wavelength.

figure-of-merits that are larger than those obtained for even the zero curvature (the flat-top nanoridge).

We specifically calculated the propagation distance and the figure-of-merit for the 120 nm wide elliptical nanoridge waveguide versus the curvature at the wavelength of 1.55 μm. The results are shown in Fig. 11. As the curvature increases, both the propagation distance and the figure-of-merit increase when the curvature is less than 9 μm^{-1}, and reach a plateau when the curvature is between 9 and 18 μm^{-1}, after which both are seen to decrease dramatically. It is concluded that for the 120 nm wide elliptical cross section silver nanoridge waveguides discussed here, the best performance can be obtained with a curvature between 9 and 18 μm^{-1} at all wavelengths, with the ultimate performance being obtained when the excitation wavelength is roughly 1.05 μm.

We also have calculated the propagation distance and the figure-of-merit for different elliptical height and nanoridge width at the 1.55 μm wavelength. The results are shown in Fig. 12. The horizontal axis is the ellipse height of the nanoridge from 0 to 1000 nm. The vertical axis is the width of the nanoridge from 50 to 500 nm. It can be seen that as the height of the elliptical ridge increases, the propagation distance and the figure-of-merit increase first, and then decrease. The white dashed lines in the Fig. 12 indicate the elliptical cross sections which become semi-circles. The propagation distance and figure-of-merit reach the maximal values along this line. This is because the plasmon mode energy is more uniformly distributed over the entire ridge, when the cross section of the nanoridge waveguide becomes a semi-circle.

III. Conclusion

Propagating plasmon modes supported by elliptical cross section silver nanoridges are investigated in this paper. We calculated the dispersion curves, propagation distances, mode sizes, and the figure-of-merits of these nanoridge plasmon modes. It is found that as the curvature of the elliptical nanoridge increases, both the propagation distance and the figure-of-merit first increase, reach a plateau, and then decrease dramatically. When the curvature falls between 9 and 18 μm^{-1} for 120 nm wide silver elliptical ridges, the ridge plasmon modes have the longest propagation distance and the highest figure-of-merit. The elliptical nanoridge waveguides with the curvature between 9 and 18 μm^{-1} have better performance in terms of the propagation distance and figure-of-merit than the flat-top nanoridge waveguides investigated previously [53]. It is found that the semi-circular cross section nanoridge waveguides, which give more uniformly mode energy distribution over the entire ridge surfaces, represent an optimal trade-off between mode confinement and propagation distance. The elliptical cross section nanoridge waveguides investigated in this paper are very desirable for applications that require large surface interaction area, such as in chemical and biological sensing.

References

[1] H. Raether, *Surface Plasmons on Smooth and Rough Surfaces and on Gratings*. Berlin, Germany: Springer-Verlag, 1988.
[2] E. A. Stern and R. A. Ferrell, "Surface plasma oscillations of a degenerate electron gas," *Phys. Rev.*, vol. 120, pp. 130–136, 1960.
[3] W. L. Barnes, A. Dereux, and T. W. Ebbesen, "Surface plasmon subwavelength optics," *Nature*, vol. 424, pp. 824–830, 2003.
[4] E. N. Economou, "Surface plasmons in thin films," *Phys. Rev.*, vol. 182, pp. 539–554, 1969.
[5] D. Sarid, "Long-range surface-plasma waves on very thin metal films," *Phys. Rev. Lett.*, vol. 47, pp. 1927–1930, 1981.
[6] A. E. Craig, G. A. Olson, and D. Sarid, "Experimental observation of the long-range surface-plasmon polariton," *Opt. Lett.*, vol. 8, pp. 380–382, 1983.
[7] G. I. Stegeman, J. J. Burke, and D. G. Hall, "Surface-polaritonlike waves guided by thin, lossy metal films," *Opt. Lett.*, vol. 8, pp. 383–385, 1983.
[8] F. Yang, J. R. Sambles, and G. W. Bradberry, "Long-range surface modes supported by thin films," *Phys. Rev. B*, vol. 44, pp. 5855–5872, 1991.

[9] R. Charbonneau, P. Berini, E. Berolo, and E. Lisicka-Shrzek, "Experimental observation of plasmon polariton waves supported by a thin metal film of finite width," *Opt. Lett.*, vol. 25, pp. 844–846, 2000.

[10] P. Berini, "Plasmon-polariton waves guided by thin lossy metal films of finite width: Bound modes of symmetric structures," *Phys. Rev. B*, vol. 61, pp. 10484–10503, 2000.

[11] B. Lamprecht, J. R. Krenn, G. Schider, H. Ditlbacher, M. Salerno, N. Felidj, A. Leitner, F. R. Aussenegg, and J. C. Weeber, "Surface plasmon propagation in microscale metal stripes," *Appl. Phys. Lett.*, vol. 79, pp. 51–53, 2001.

[12] R. Zia, A. Chandran, and M. L. Brongersma, "Dielectric waveguide model for guided surface polaritons," *Opt. Lett.*, vol. 30, pp. 1473–1475, 2005.

[13] A. Degiron and D. Smith, "Numerical simulations of long-range plasmons," *Opt. Exp.*, vol. 14, pp. 1611–1625, 2006.

[14] P. Berini, "Plasmon-polariton modes guided by a metal film of finite width bounded by different dielectrics," *Opt. Exp.*, vol. 7, pp. 329–335, 2000.

[15] P. Berini, "Long-range surface plasmon-polariton waveguides in silica," *J. Appl. Phys.*, vol. 102, pp. 053105–053108, 2007.

[16] S. J. Al-Bader, "Optical transmission on metallic wires-fundamental modes," *IEEE J. Quantum Electron.*, vol. 40, no. 3, pp. 325–329, Mar. 2004.

[17] P. Berini, "Plasmon polariton modes guided by a metal film of finite width," *Opt. Lett.*, vol. 24, pp. 1011–1013, 1999.

[18] J. Q. Lu and A. A. Maradudin, "Channel plasmons," *Phys. Rev. B*, vol. 42, pp. 11159–11165, 1990.

[19] I. V. Novikov and A. A. Maradudin, "Channel polaritons," *Phys. Rev. B*, vol. 66, 2002, Art. ID 035403.

[20] D. K. Gramotnev and D. F. P. Pile, "Single-mode subwavelength waveguide with channel plasmon-polaritons in triangular grooves on a metal surface," *Appl. Phys. Lett.*, vol. 85, pp. 6323–6325, 2004.

[21] D. F. P. Pile and D. K. Gramotnev, "Channel plasmon-polariton in atriangular groove on a metal surface," *Opt. Lett.*, vol. 29, pp. 1069–1071, 2004.

[22] S. I. Bozhevolnyi, V. S. Volkov, E. Devaux, and T. W. Ebbesen, "Channel plasmon-polariton guiding by subwavelength metal grooves," *Phys. Rev. Lett.*, vol. 95, 2005, Art. ID 046802.

[23] S. I. Bozhevolnyi, "Effective-index modeling of channel plasmon polaritons," *Opt. Exp.*, vol. 14, pp. 9467–9476, 2006.

[24] E. Moreno, F. J. Garcia-Vidal, S. G. Rodrigo, L. Martin-Moreno, and S. I. Bozhevolnyi, "Channel plasmon-polaritons: Modal shape, dispersion, and losses," *Opt. Lett.*, vol. 31, pp. 3447–3449, 2006.

[25] E. Feigenbaum and M. Orenstein, "Modeling of complementary (void) plasmon waveguiding," *J. Lightw. Technol.*, vol. 25, no. 9, pp. 2547–2562, Sep. 2007.

[26] M. Yan and M. Qiu, "Guided plasmon polariton at 2-D metal corners," *J. Opt. Soc. Amer. B*, vol. 24, pp. 2333–2342, 2007.

[27] Y. Satuby and M. Orenstein, "Surface plasmon-polariton modes in deep metallic trenches—Measurement and analysis," *Opt. Exp.*, vol. 15, pp. 4247–4252, 2007.

[28] L. Liu, Z. Han, and S. He, "Novel surface plasmon waveguide for high integration," *Opt. Exp.*, vol. 13, pp. 6645–6650, 2005.

[29] G. Veronis and S. Fan, "Modes of subwavelength plasmonic slot waveguides," *J. Lightw. Technol.*, vol. 25, no. 9, pp. 2511–2521, Sep. 2007.

[30] L. Wendler and R. Haupt, "Long-range surface plasmon-polaritons in asymmetric layer structures," *J. Appl. Phys.*, vol. 59, pp. 3289–3291, 1986.

[31] J. Guo and R. Adato, "Extended long range plasmon waves in finite thickness metal film and layered dielectric materials," *Opt. Exp.*, vol. 14, pp. 12409–12418, 2006.

[32] R. Adato and J. Guo, "Novel metal-dielectric structures for guiding ultra-long-range surface plasmon-polaritons at optical frequencies," in *Proc. SPIE*, 2007, pp. 66410G–66418.

[33] J. Guo and R. Adato, "Control of 2-D plasmon-polariton mode with dielectric nanolayers," *Opt. Exp.*, vol. 16, pp. 1232–1237, 2008.

[34] Z. Sun, "Vertical dielectric-sandwiched thin metal layer for compact, low-loss long range surface plasmon waveguiding," *Appl. Phys. Lett.*, vol. 91, pp. 111112–111113, 2007.

[35] F. Y. Kou and T. Tamir, "Range extension of surface plasmons by dielectric layers," *Opt. Lett.*, vol. 12, pp. 367–369, 1987.

[36] Y. Wang, R. Islam, and G. V. Eleftheriades, "An ultra-short contra-directional coupler utilizing surface plasmon-polaritons at optical frequencies," *Opt. Exp.*, vol. 14, pp. 7279–7290, 2006.

[37] R. Adato and J. Guo, "Characteristics of ultra-long range surface plasmon waves at optical frequencies," *Opt. Exp.*, vol. 15, pp. 5008–5017, 2007.

[38] J. Chen, G. A. Smolyakov, S. R. Brueck, and K. J. Malloy, "Surface plasmon modes of finite, planar, metal-insulator-metal plasmonic waveguides," *Opt. Exp.*, vol. 16, pp. 14902–14909, 2008.

[39] R. Adato and J. Guo, "Modification of dispersion, localization, and attenuation of thin metal stripe symmetric surface plasmon-polariton modes by thin dielectric layers," *J. Appl. Phys.*, vol. 105, pp. 034306–034311, 2009.

[40] A. V. Krasavin and A. V. Zayats, "Passive photonic elements based on dielectric-loaded surface plasmon polariton waveguides," *Appl. Phys. Lett.*, vol. 90, pp. 211101–211103, 2007.

[41] B. Steinberger, A. Hohenau, H. Ditlbacher, A. L. Stepanov, A. Drezet, F. R. Aussenegg, A. Leitner, and J. R. Krenn, "Dielectric stripes on gold as surface plasmon waveguides," *Appl. Phys. Lett.*, vol. 88, pp. 094104–094103, 2006.

[42] T. Holmgaard, Z. Chen, S. I. Bozhevolnyi, L. Markey, A. Dereux, A. V. Krasavin, and A. V. Zayats, "Bend- and splitting loss of dielectric-loaded surface plasmon-polariton waveguides," *Opt. Exp.*, vol. 16, pp. 13585–13592, 2008.

[43] A. V. Krasavin and A. V. Zayats, "Three-dimensional numerical modeling of photonic integration with dielectric-loaded SPP waveguides," *Phys. Rev. B*, vol. 78, 2008, Art. ID 045425.

[44] C. Reinhardt, A. Seidel, A. B. Evlyukhin, W. Cheng, and B. N. Chichkov, "Mode-selective excitation of laser-written dielectric-loaded surface plasmon polariton waveguides," *J. Opt. Soc. Amer. B*, vol. 26, pp. B55–B60, 2009.

[45] A. V. Krasavin and A. V. Zayats, "Silicon-based plasmonic waveguides," *Opt. Exp.*, vol. 18, pp. 11791–11799, 2010.

[46] I. I. Smolyaninov, Y.-J. Hung, and C. C. Davis, "Surface plasmon dielectric waveguides," *Appl. Phys. Lett.*, vol. 87, pp. 241106–241103, 2005.

[47] A. D. Boardman, G. C. Aers, and R. Teshima, "Retarded edge modes of a parabolic wedge," *Phys. Rev. B*, vol. 24, pp. 5703–5712, 1981.

[48] J. A. Sánchez-Gil, "Localized surface-plasmon polaritons in disordered nanostructured metal surfaces: Shape versus Anderson-localized resonances," *Phys. Rev. B*, vol. 68, 2003, Art. ID 113410.

[49] D. F. P. Pile, T. Ogawa, D. K. Gramotnev, T. Okamoto, M. Haraguchi, M. Fukui, and S. Matsuo, "Theoretical and experimental investigation of strongly localized plasmons on triangular metal wedges for subwavelength waveguiding," *Appl. Phys. Lett.*, vol. 87, pp. 061106–061103, 2005.

[50] E. Feigenbaum and M. Orenstein, "Nano plasmon polariton modes of a wedge cross section metal waveguide," *Opt. Exp.*, vol. 14, pp. 8779–8784, 2006.

[51] E. Moreno, S. G. Rodrigo, S. I. Bozhevolnyi, L. Martín-Moreno, and F. J. García-Vidal, "Guiding and focusing of electromagnetic fields with wedge plasmon polaritons," *Phys. Rev. Lett.*, vol. 100, 2008, Art. ID 023901.

[52] E. J. R. Vesseur, R. de Waele, H. J. Lezec, H. A. Atwater, F. J. G. de Abajo, and A. Polman, "Surface plasmon polariton modes in a single-crystal Au nanoresonator fabricated using focused-ion-beam milling," *Appl. Phys. Lett.*, vol. 92, pp. 083110–083113, 2008.

[53] Z. Pan, J. Guo, R. Soref, W. Buchwald, and G. Sun, "Mode properties of flat-top silver nanoridge surface plasmon waveguides," *J. Opt. Soc. Amer. B*, vol. 29, pp. 340–345, 2012.

[54] Z. Pan, J. Guo, R. Soref, W. Buchwald, and G. Sun, "Guided plasmon modes of triangular and inverted triangular cross section silver nanoridges," *J. Opt. Soc. Amer. B*, vol. 29, pp. 950–958, 2012.

[55] X. Luo, J. Sun, J. Ritchie, W. Chang, and W. Wang, "Deterministic fabrication of nanostructures for plasmonic lens by focused ion beam," *Int. J. Adv. Manuf. Technol.*, vol. 57, pp. 1003–1009, 2011.

[56] P. B. Z. Johnson, Zhaoming, R. W. B. Christy, and Thomas, "Optical constants full-vectorial finite-difference analysis of the noble metals microstructured optical fibers," *Phys. Rev. B*, vol. 610, pp. 4379853–4379864, 2002.

[57] P. B. Johnson and R. W. Christy, "Optical constants of the noble metals," *Phys. Rev. B*, vol. 6, pp. 4370–4379, 1972.

[58] R. Soref, R. E. Peale, and W. Buchwald, "Longwave plasmonics on doped silicon and silicides," *Opt. Exp.*, vol. 16, pp. 6507–6514, 2008.

[59] J. W. Cleary, R. E. Peale, D. J. Shelton, G. D. Boreman, C. W. Smith, M. Ishigami, R. Soref, A. Drehman, and W. R. Buchwald, "IR permittivities for silicides and doped silicon," *J. Opt. Soc. Amer. B*, vol. 27, pp. 730–734, 2010.

[60] S.-Y. Cho and R. A. Soref, "Low-loss silicide/silicon plasmonic ribbon waveguides for mid and far-infrared applications," *Opt. Lett.*, vol. 34, pp. 1759–1761, 2009.
[61] R. Zia, M. D. Selker, P. B. Catrysse, and M. L. Brongersma, "Geometries and materials for subwavelength surface plasmon modes," *J. Opt. Soc. Amer. A*, vol. 21, pp. 2442–2446, 2004.
[62] P. Berini, "Figures of merit for surface plasmon waveguides," *Opt. Exp.*, vol. 14, pp. 13030–13042, 2006.
[63] R. Buckley and P. Berini, "Figures of merit for 2-D surface plasmon waveguides and application to metal stripes," *Opt. Exp.*, vol. 15, pp. 12174–12182, 2007.

Zeyu Pan (S'12) received the B.S. degree in optical information science and technology from Nanjing University of Science and Technology, Nanjing, China, in 2010. He is currently working toward the M.S. degree at the University of Alabama, Huntsville.

His research interests include the nanoplasmonic waveguide, extraordinary optical transmission, nonlinear optics, and electromagnetic algorithms.

Junpeng Guo received the M.S. degree in nuclear plasma engineering and Ph.D. degree in electrical engineering from the University of Illinois at Urbana-Champaign.

He is currently an Associate Professor of electrical engineering and an Associate Professor of optical science and engineering with the University of Alabama, Huntsville. After his graduation from the Illinois, he became a Research Scientist with the former Rockwell Science Center, Thousand Oaks, CA, and later as a Member of Technical Staff with the Sandia National Laboratories, Albuquerque, NM. He has worked in numerous research areas in photonics, optics, and lasers. Most notably, he made the first thin-film micro-polarizer array for polarization imaging and 3-D displays. His current research interests are plasmonics, nanophotonics, and metamaterials.

Richard Soref (LF'03) received the Ph.D. degree in electrical engineering from Stanford University, Stanford, CA, in 1963.

He is currently a Research Professor at the University of Massachusetts at Boston. His research career in electrooptics spans 48 years.

Dr. Soref is a Fellow of the Optical Society of America, the Air Force Research Laboratory, and the Institute of Physics UK. In 2007, he received the Lifetime Achievement Award from the IEEE Photonics Society's International Conference on Group IV Photonics.

Walter Buchwald received the M.S. degree in physics, the M.S. degree in electrical engineering, and the Ph.D. degree.

He is currently the Director of Research for Solid State Scientific Corporation, Nashua, New Hampshire. He has held a variety of technical positions investigating semiconductor materials, devices, and advanced fabrication techniques at the Army Research Laboratory, the Raytheon Advanced Device Center, Axsun Technologies and most recently with the Air Force Research Laboratory where he initiated programs in plasmonics and IR integrated quantum optics. He has authored and coauthored over 90 publications and holds two patents and is a graduate faculty scholar with the Physics Department of the University of Central Florida.